Terahertz magnetization dynamics induced by femtosecond resonant pumping of Dy³⁺ subsystem in the multisublattice antiferromagnet DyFeO₃

R. V. Mikhaylovskiy,[1] T. J. Huisman,[1] A. I. Popov,[2] A. K. Zvezdin,[3,4,5] Th. Rasing,[1] R. V. Pisarev,[6] and A. V. Kimel[1,4]

[1]*Radboud University, Institute for Molecules and Materials, 6525 AJ Nijmegen, The Netherlands*
[2]*National Research University of Electronic Technology, 124498 Zelenograd, Russia*
[3]*Prokhorov General Physics Institute, Russian Academy of Sciences, 119991 Moscow, Russia*
[4]*Moscow State Technical University of Radio Engineering, Electronics, and Automation, 119454 Moscow, Russia*
[5]*Moscow Institute of Physics and Technology (MFTI), 141700 Moscow Region, Russia*
[6]*Ioffe Physical Technical Institute, 194021 St. Petersburg, Russia*

Resonant optical pumping of $f - f$ electronic transitions in the Dy³⁺ subsystem with femtosecond laser pulses in the multisublattice antiferromagnet DyFeO₃ produces a strongly pronounced effect on the induced magnetization dynamics. Analyzing the polarization and spectral properties of the emitted THz radiation, we infer that the resonant pumping magnetizes the partially ordered Dy³⁺ ions on a femtosecond time scale with the induced longitudinal change of the magnetization reaching almost 1%. We also show that for laser photon energies close to the $f - f$ resonance of Dy³⁺ ions, a minimum in the efficiency of spin-wave excitation in the Fe³⁺ subsystem via the inverse Faraday effect is observed. This observation reveals that the resonant photo-induced magnetization in the Dy³⁺ subsystem and the off-resonant excitation of spin waves in the Fe³⁺ subsystem are intrinsically competing processes.

PACS number(s): 78.47.D−, 78.20.Ls, 78.47.J−, 78.66.Nk

I. INTRODUCTION

Manipulation of magnetic order using femtosecond laser pulses is an intriguing topic of fundamental science [1] which may have implications in the areas of spintronics [2], magnonics [3], and multiferroics [4]. The action of the electric field of light on electronic charges, which is the largest perturbation in the physics of light-matter interaction, conserves the electron spin. This is why the seminal observation of subpicosecond demagnetization in metallic ferromagnetic nickel by a 60 fs laser pulse [5] immediately triggered intense debate about the mechanisms allowing ultrafast and effective control of spins by light in condensed matter.

Dielectric materials appeared to be an excellent playground in which to study these mechanisms. Unlike metals, the electronic structure of dielectrics is well defined due to the presence of strongly localized states. This fact allows one to trace how and how fast selective pumping of specific electronic excitations result in magnetic changes. For instance, an effective coupling of visible light to spins can be achieved via off-resonant optical excitation of magnetic ions [6]. Phenomenologically, such a coupling can be described in terms of the inverse Faraday and Cotton-Mouton effects [7], which appear to be very general and have been demonstrated in various classes of magnetic dielectrics including transition-metal oxides [8–17] and fluorides [18]. Although many of these compounds contain rare-earth 4f ions, their multisublattice nature has often been ignored and all of these findings have been described in terms of off-resonant femtosecond pumping of the 3d transition-metal ions (Mn, Fe, Co, Ni).

Recently, using the example of hexagonal multiferroic ErMnO₃, it has been shown that due to a hybridization between magnetic dipole spin waves in the Mn³⁺ subsystem and the low-energy (THz range) electric dipole crystal-field excitations of the rare-earth Er³⁺ ions, the Mn³⁺ spin waves can be excited indirectly via resonant THz pumping of the Er³⁺ subsystem [19]. Note that electric dipole crystal-field transitions in rare-earth ions are also present at much higher than THz frequencies in the near-infrared and visible ranges and thus can be potentially addressed at much shorter time scales [20]. Here we explore and analyze the magnetization dynamics of rare-earth ions triggered by femtosecond resonant excitation and the role of such a resonant pumping in ultrafast optical control of magnetic order in multisublattice magnetic insulators.

We address these issues for the case of the multisublattice antiferromagnet DyFeO₃ using spectrally tunable 40 fs circularly polarized pump pulses and detect the laser-induced magnetization with the help of THz emission spectroscopy. The paper is organized as follows. Section II discusses details of the studied sample and the experimental setup. Section III describes experimental results and suggests their interpretation. The paper is concluded with Sec. IV.

II. STUDIED MATERIAL AND EXPERIMENTAL PROCEDURE

In the rare-earth orthoferrites RFeO₃ (R is a rare-earth ion), the spins of Fe³⁺ ions are coupled antiferromagnetically and retain their order up to about 645 K. In DyFeO₃ above the Morin point, $T_M \approx 41$ K, the iron spins are aligned along the a axis and, due to the Dzyaloshinskii-Moriya interaction, the opposite spins acquire a canting over an angle of about 0.5°, giving rise to a small spontaneous magnetization M_S^{Fe} along the c axis [see Fig. 1(a)]. The Dy-magnetic moments are not ordered above 4 K. At $T > T_M$, due to the $d - f$ exchange interaction, the magnetization M_S^{Fe} acts on the Dy³⁺ ions as an effective magnetic field and magnetizes the rare-earth ions along the c axis, increasing the net magnetization $M_S = M_S^{Fe} + M_S^{Dy}$, where M_S^{Dy} is the magnetization of the Dy sublattice.
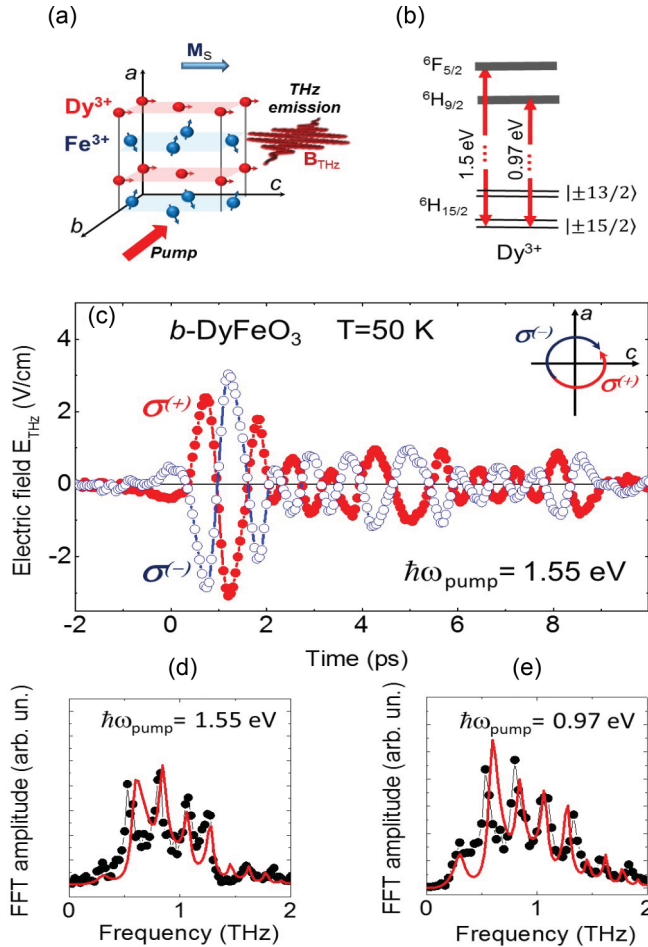
FIG. 1. (Color online) (a) Magnetic structure of $DyFeO_3$ in relation to the geometry of the experiment. Large and small balls represent the Fe^{3+} and Dy^{3+} ions, respectively. The Fe^{3+} spins are aligned along the a axis, while due to the Dzyaloshinskii-Moriya interaction the spins are canted and the crystal acquires a net magnetic moment $\mathbf{M}_S$ along the c axis. The spins of Dy^{3+} are partially aligned in the direction of $\mathbf{M}_S^{Fe}$ due to the $d-f$ exchange interaction. (b) Particular details of the electronic structure of Dy^{3+} ions. (c) Temporal evolution of the electric field of the THz radiation triggered by 40 fs circularly polarized pulses of opposite helicities. $\sigma^{(+)}$ (filled circles) and $\sigma^{(-)}$ (open circles) correspond to the right- and left-handed circularly polarized pump, respectively. The temperature of the sample is $T = 50$ K. The central photon energy of the pump is $\hbar\omega = 1.55$ eV. (d) Fourier-transform spectrum of the time dependence shown in (c) (filled circles). The central photon energy of the pump is $\hbar\omega = 1.55$ eV. The red solid line is the calculated spectrum. (e) Fourier-transform spectrum of the THz radiation for the pump with the central photon energy $\hbar\omega = 0.97$ eV. The red solid line is the calculated spectrum.

Interaction of the near-infrared and visible light with $DyFeO_3$ is defined by localized transitions in Fe^{3+} and Dy^{3+} ions. In this spectral range, Fe^{3+} ions are characterized by two weak $d-d$ transitions at the energies of 1.2 and 1.8 eV [21]. The local symmetry of the Dy^{3+} ions in $DyFeO_3$ is described by the point group C_S so that the original ground-state multiplet $^6H_{15/2}$ ($L = 5$, $S = 5/2$, $J = 15/2$), corresponding to that of the Dy^{3+} ion, splits and the lowest two

doublets with a good accuracy are $|\pm15/2\rangle$ ($M_J = \pm15/2$) and $|\pm13/2\rangle$ ($M_J = \pm13/2$) [22]. Since the Dy^{3+} ions are located in noncentrosymmetric positions, otherwise forbidden optical transitions become allowed in the electric dipole approximation, including the transition between H and F states: from $^6H_{15/2}$ to $^6F_{5/2}$ ($L = 3$, $S = 5/2$, $J = 5/2$) around 1.5 eV and from $^6H_{15/2}$ to $^6H_{9/2}$ ($L = 5$, $S = 5/2$, $J = 9/2$) around 0.97 eV [see Fig. 1(b)].

The studied $DyFeO_3$ crystal was cut perpendicular to the b crystallographic axis and had the thickness of $d = 100$ μm. The pump had a fluence of about 1 mJ/cm^2, being focused into a spot with the diameter of 2 mm. Pico- and subpicosecond magnetization dynamics must be accompanied by magnetic-dipole emission of the electromagnetic radiation in the THz spectral range. Searching for such an emission, we performed time-resolved detection of the THz radiation. For the measurements, we used a THz spectrometer similar to those described elsewhere [23–27], which allowed us to measure the electric field of the emitted THz radiation as a function of time. Our experiments were performed in an external magnetic field ± 1 kG applied along the c axis sufficient to saturate the magnetization. The measurements were performed above the Morin point, $T \geqslant 50$ K, where the sample can be easily brought into a single domain state with the help of an external magnetic field.

III. EXPERIMENTAL RESULTS AND DISCUSSION

A. Broadband THz emission

The time traces of the electric field E of the radiation emitted by the $DyFeO_3$ sample after pumping it by a circularly polarized 40 fs laser pulse with the central photon energy of 1.55 eV are shown in Fig. 1(c). The signal has the form of a single-cycle pulse with an oscillatory tail. Fourier transform of the signals reveals that the traces correspond to electromagnetic radiation in the THz spectral range [see Fig. 1(d)]. This is a broadband spectrum with a width of $\approx$ 1 THz with superimposed fine structure of nearly equidistant peaks. These peaks are due to the multiple reflection of the single-cycle THz pulse from the sample interfaces. Changing the helicity of the circular polarization of the pump leads to the sign change of the THz field. The emitted THz radiation is linearly polarized with the E field along the a axis of the sample. The electric field of the emitted radiation is found to scale linearly with the intensity of the pump pulse. The measurements with the pump having a central photon energy of 0.97 eV led to very similar results and the spectrum of the emitted radiation is shown in Fig. 1(e).

The measured broadband THz emission has rather unconventional properties that are proportional to the degree of ellipticity of the pump polarization. Such a behavior indicates the decisive role of the angular momentum of the pump photons in the process leading to the THz emission. The source of the emitted THz radiation can be either an electric polarization $p_a(t)$ lying along the a axis or a magnetization $m_c(t)$ along the c axis, varying in time at a subpicosecond scale.

$DyFeO_3$ crystals are characterized by a centrosymmetric space group $D_{2h}^{16}(Pbnm)$ and, in the electric dipole approximation, a generation of the electric polarization $p_a(t)$ linear
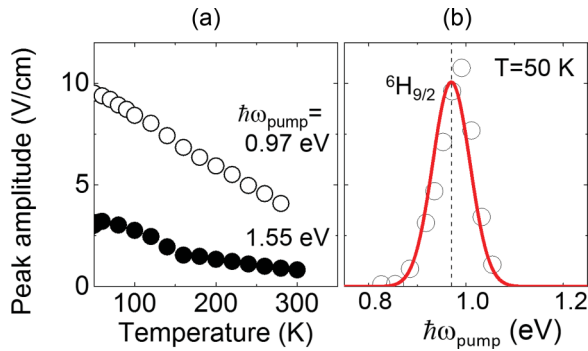
FIG. 2. (Color online) (a) Temperature dependence of the peak amplitude of the THz signal triggered by the pumps with the central photon energy $\hbar\omega = 1.55$ eV (filled circles) and $\hbar\omega = 0.97$ eV (open circles), respectively. (b) The peak amplitude of the THz radiation as a function of the central photon energy of the pump. The solid line is the fit by a Gaussian function.

with respect to the intensity of the pump is forbidden [28]. Phenomenologically, the THz generation is very similar to second-harmonic generation, which during recent years has been intensively studied in magnetic materials [29]. The effect of polarization of light on the second harmonic has been recognized to be a rather intriguing phenomenon, but has not obtained much attention so far [30,31]. It is known that circularly polarized light can induce magnetization in the media of any symmetry [7,32]. In particular, it was reported that light can induce magnetization in a medium by pumping Ce ions [33]. For THz emission which arises from such a resonant optical excitation of magnetization in rare-earth ions, we suggest that the source of the THz radiation is the photo-induced magnetization $m_c(t)$. Note that the net spontaneous magnetization M_S of $DyFeO_3$ is aligned along the c axis as well.

Temperature dependencies of the peak THz electric field measured for the pump pulses centered at 1.55 and 0.97 eV reveal a decrease of its amplitude upon heating [see Fig. 2(a)]. Each of these dependencies is in a good qualitative agreement with the temperature dependence of the net magnetic moment M_S of $DyFeO_3$ along the c axis, which originates from temperature dependence of the paramagnetic susceptibility of the Dy^{3+} ions in the direction of the c axis (see [34]). Measurements of the peak amplitude of the emitted THz radiation as a function of the central photon energy of the pump reveal a strong resonance at the energy of the transition from the $^6H_{15/2}$ manifold to the $^6H_{9/2}$ manifold [see Fig. 2(b)]. All of these experimental findings strongly suggest that the THz emission from $DyFeO_3$ is due to electronic transitions in Dy^{3+} ions which eventually lead to the laser-induced magnetization $m_c(t)$.

Phenomenologically, the light-induced magnetization in the frequency domain can be described as $m_\alpha = \chi^{(m)}_{\alpha\beta\gamma} E_\beta(\omega) E^*_\gamma(\omega)$, where $\chi^{(m)}_{\alpha\beta\gamma}$ is an axial tensor of a third rank, E_β is the electric field of light along the β axis at the frequency ω, and E^*_γ is the complex conjugate of the electric field of the pump along the γ axis. The space group of the orthoferrite dictates that in order to induce the magnetization

along the c axis, the electric field of light should have nonzero components along both the a and b axes.

We did not reveal any effect of the polarity of the bias magnetic field on the emitted THz radiation [see Fig. 3(a)]. Rotating the crystal around the a axis over $180°$ did not affect the THz emission either [see Fig. 3(b)]. Finally, we have rotated the sample around the b axis and found that the rotation of $180°$ reverses the sign of the THz electric field [see Fig. 3(c)]. All of these observations are in agreement with the hypothesis stating that the source of the THz emission is photo-induced magnetization along the c axis.

Note that orthoferrites are optically anisotropic materials with two optic axes lying in the bc plane [35]. Even if the incident wave before entering the medium propagates along the normal to the samples boundary, inside the medium the wave vector and the electric field of light are not orthogonal so that $E_b(\omega) \neq 0$. Thus, the photo-induced magnetization along the c axis is allowed and $m_c \neq 0$. Note that either tilting the sample around the a or around the b axis over a small angle of less than $10°$ only slightly changed the intensity of the THz emission, but did not lead to its complete disappearance. This fact shows that the observed phenomenon cannot be explained just by a miscut or misalignment of the crystal axes.

B. Narrowband THz emission

The magnetization $m_c(t)$ induced along the c axis of the sample by a resonant pumping of Dy^{3+} ions could launch Fe^{3+} spin waves via a mechanism different from the off-resonant inverse Faraday effect. To reveal whether this mechanism of optomagnetic excitation of the Fe^{3+} spin waves does really take place and how it affects the total efficiency of the spin-wave excitation, we performed the measurements over a longer time domain at room temperature where the quasiantiferromagnetic mode has the highest frequency of about 500 GHz [36]. First, the measurements were performed for the case of off-resonant excitation $\hbar\omega = 0.8$ eV, where the resonant mechanism discussed above is not effective and the spin resonances can be excited via the off-resonant inverse Faraday effect. It is seen that both right- and left-handed circularly polarized pump pulses trigger oscillations, in which the phase depends on the helicity of the pump [see Fig. 4(a)]. Fourier transform of the time dependencies reveals that the frequency of the oscillations corresponds to the one of antiferromagnetic resonance [see Fig. 4(b)]. Note that apart from the helicity-dependent effects discussed here, polarization-independent excitation of the spin waves was also observed, but falls beyond the scope of this paper [37,38].

We calculated the amplitude of the helicity-dependent part of the oscillations as a difference between the measurements performed for the two opposite helicities of the pump and plotted the amplitude of the helicity-dependent part as a function of the pump photon energy. The result is shown in Fig. 4(c). It is seen that the amplitude of the spin oscillations substantially drops at the energy of the transitions from the $^6H_{15/2}$ state to the $^6H_{9/2}$ state. This observation suggests that the resonant photo-induced magnetization of the Dy^{3+} and the off-resonant excitation of the Fe^{3+} spin waves via the inverse Faraday effect are competing processes. Indeed, the absorption
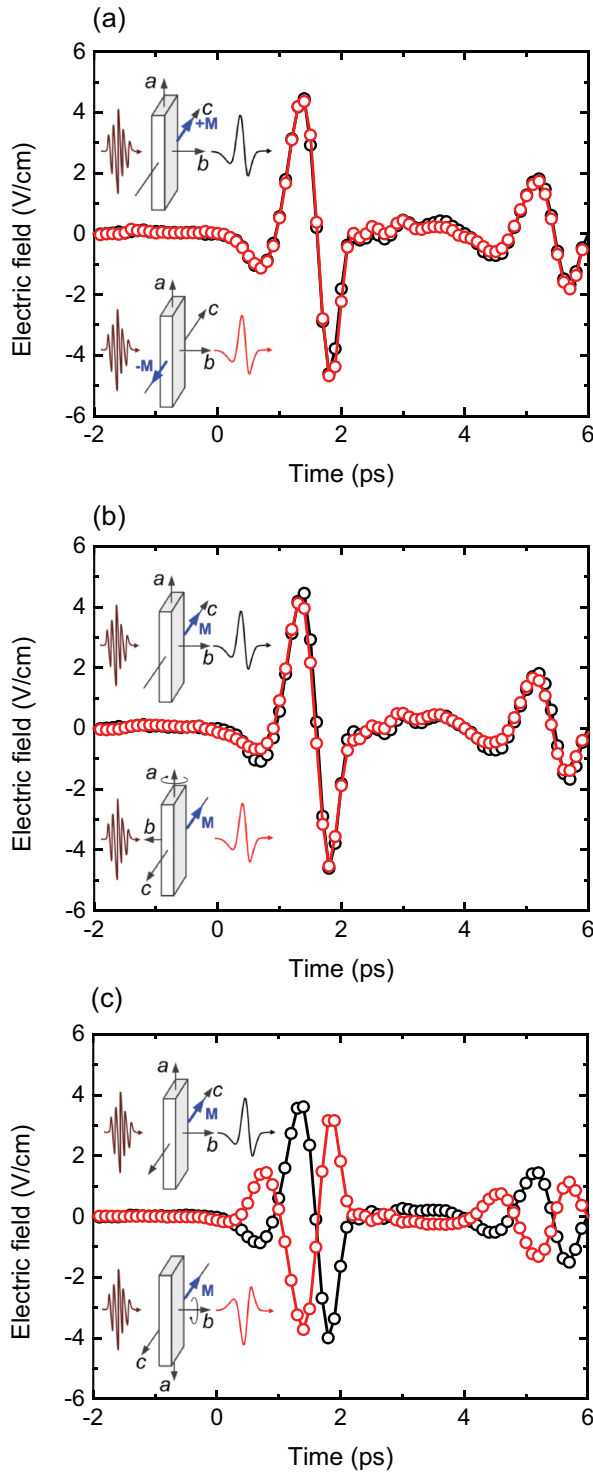
FIG. 3. (Color online) The THz emission in different experimental geometries. (a) THz emission as a function of the direction of the magnetization along the *c* axis. (b) Sensitivity of the THz emission to rotation of the sample around the *a* axis. (c) Sensitivity of the THz emission to rotation of the sample around the *b* axis. All measurements were conducted for the same helicity of the pump light with the wavelength 1300 nm (photon energy 0.95 eV) at room temperature. The magnetization was flipped with the reversal of the bias field polarity for the fixed orientation. While the sample was rotated, the bias magnetic field was applied along the same direction to ensure the orientation of the magnetization is fixed.
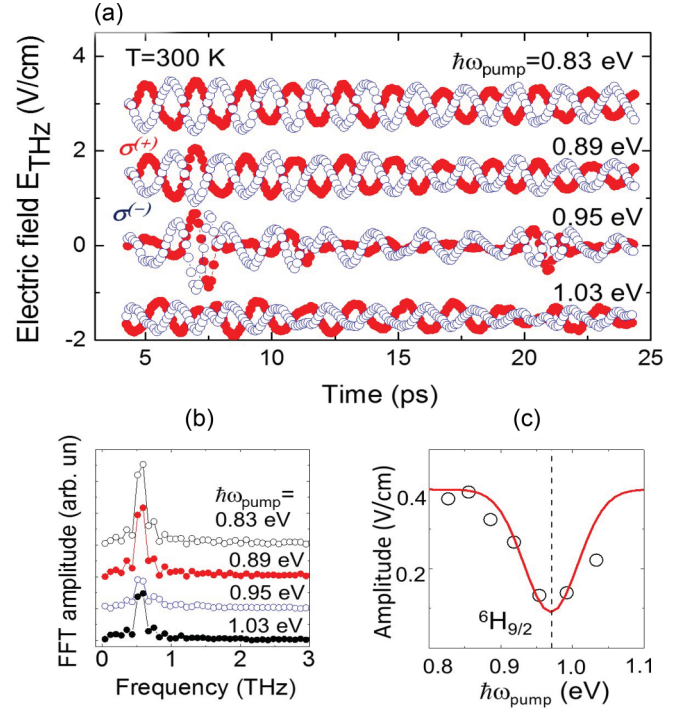

FIG. 4. (Color online) (a) Temporal evolution of the electric field of the THz radiation triggered by 40 fs circularly polarized pulses of opposite helicities. $\sigma^{(+)}$ (filled circles) and $\sigma^{(-)}$ (open circles) correspond to the right- and left-handed circularly polarized pump, respectively. To focus on narrowband emission at the frequency of the antiferromagnetic resonance, the measurements have been done in a time window from 5 to 25 ps. The temperature of the sample was $T = 300$ K. (b) Fourier-transform spectrum of the time dependence shown in Fig. 3(a). (c) The amplitude of the helicity-dependent part at the frequency of antiferromagnetic resonance as a function of the central photon energy of the pump. The helicity-dependent part was deduced performing the measurements for two opposite helicities of the circularly polarized pump and taking the difference between them. The solid line is the Gaussian function with the central frequency and the dispersion taken from the fit in Fig. 2(b).

of light by the Dy^{3+} ions at the energy of the resonance decreases the probability of off-resonant Raman scattering of light responsible for the Fe^{3+} spin-wave excitations. Moreover, this drop in efficiency can also be understood as a result of destructive interference. In particular, it can be explained if the magnetization, induced via a resonant pumping of the rare-earth ions, launches Fe^{3+} spin waves out of phase with those launched via other off-resonant mechanisms.

C. Modeling of the photo-induced magnetization

To verify the adequacy of the aforementioned assumption, we performed calculations using the Bloch equations for a two-level system,

$$\frac{dp(t)}{dt} + \left(\frac{1}{T_2} + i\omega_0\right)p(t) + \frac{i}{\hbar}DE(t)[1 - 2N(t)] = 0, \quad (1)$$

$$\frac{dN(t)}{dt} + \frac{1}{T_1}N(t) + \frac{i}{\hbar}[DE(t)p^*(t) - DE^*(t)p(t)] = 0, \quad (2)$$
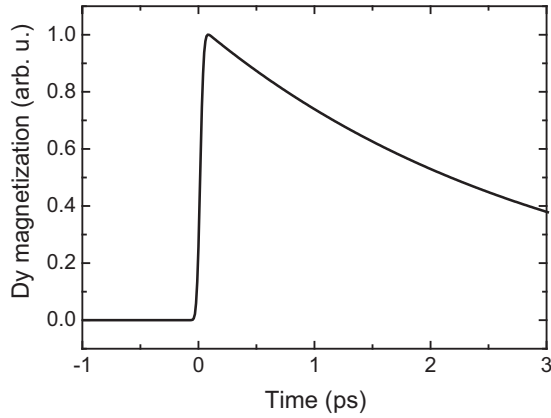
FIG. 5. Temporal profile of the population of the excited state $N(t)$ induced by the Gaussian 40 fs laser pulses at the central wavelength 1275 nm (photon energy 0.97 eV).

where $p(t)$ describes the off-diagonal components of the density matrix which determine polarization, while $N(t)$ is the population of the excited state. Here the optical field $E(t) = \varepsilon(t)e^{-i\omega t}$ has a Gaussian envelope, $\varepsilon(t) = E_0 \exp(-t^2/\tau^2)$, where τ is the laser-pulse duration, while T_1 and T_2 are the lifetime and dephasing time, respectively, D is the electric dipole moment of the transition, and ω_0 denotes the resonance frequency.

We also assume that the change of the magnetization of the two-level system is proportional to the population of the excited state in the two-level system, $m_c(t) = 2N(t)(\mu_{22} - \mu_{11})$, where μ_{11} and μ_{22} are the magnetic moments along the c axis of the ground and excited states, respectively. Since the effect of interest scales linearly with the pump intensity, we calculate $N(t)$ proportional to the square of the electric-field amplitude of the pump E_0.

To calculate $N(t)$, we take the pulse duration $\tau = 40$ fs and $T_1 = T_2 \approx 3$ ps that is inferred from the Dy absorption bands [39]. However, it should be noted that since $\tau \ll T_1$, the THz emission calculated with the help of this model hardly depends on T_1. The calculations with a longer time give similar results. The resulting function $N(t)$, which defines the magnetization, is shown in Fig. 5. One can see from this figure that the resonant pumping results in the population of the excited state on the femtosecond time scale, which is followed by a slower relaxation on the picosecond time scale.

Further, we calculated the spectrum of the electric field emitted into free space by the magnetization $m(t)$ propagating inside the sample with the group velocity of the pump pulse. For the calculation, we have chosen a rectangular coordinate system of x, y, and z axes which correspond to a, b, and c axes of the orthorhombic crystal, respectively:

$$\mathbf{m}(t,y) = m_0 N\left[t - \frac{(y+d)}{V}\right] \exp[-(y+d)/l][\Theta(y+d)$$
$$- \Theta(y)]\mathbf{z}_0, \qquad (3)$$

where m_0 is the amplitude, the y axis corresponds to the light-propagation direction, $\mathbf{z}_0$ is the unit vector along the z axis, and Θ is the Heaviside step function. V is the group velocity of the pump and l is the characteristic optical penetration depth.
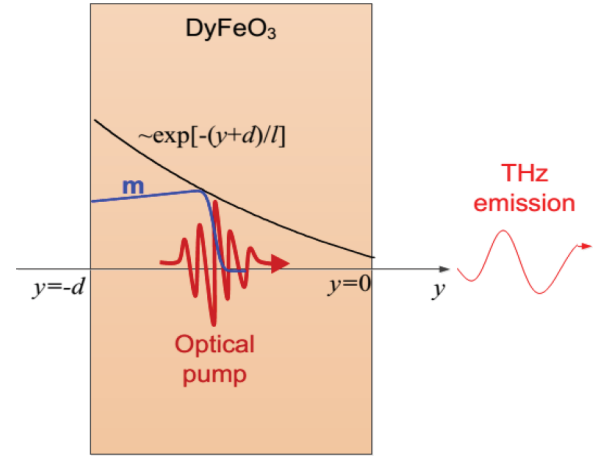

FIG. 6. (Color online) The optical pulse propagates inside the sample with thickness d and induces the transient magnetization **m**. The magnetization follows the laser pulse and propagates with its group velocity. The intensity of the laser pulse and hence the amplitude of the transient magnetization exponentially decay along the propagation direction.

The spatial distribution of the magnetization across the slab is illustrated in Fig. 6.

To find the emitted electric field, we solve the wave equation in the frequency domain,

$$\frac{\partial^2 \tilde{E}_x(\omega,y)}{\partial^2 y} + \frac{\omega^2}{c^2}n^2 \tilde{E}_x(\omega,y) = -\frac{4\pi}{c}i\omega\frac{\partial \tilde{m}_z(\omega,y)}{\partial y}, \qquad (4)$$

where the wavy line above the symbols denotes the Fourier transforms. The refractive index $n(y)$ in the THz range is equal to n_s within the sample ($-d < y < 0$) and unity outside of it. Taking into account Eq. (3), we get

$$\frac{\partial \tilde{m}_z(\omega,y)}{\partial y} = m_0 \tilde{N}(\omega)[\delta(y+d) - \delta(y)]\exp\left(-\frac{y+d}{\Lambda}\right)$$
$$- \frac{1}{\Lambda}[\Theta(y+d) - \Theta(y)]\exp\left(-\frac{y+d}{\Lambda}\right), \qquad (5)$$

where $\Lambda = \frac{lV}{V+i\omega l}$ and $\delta(y)$ is the Dirac delta function. We solve Eq. (4) in the homogeneous regions $y < -d$, $-d < y < 0$, and $y > 0$, matching the solutions by the boundary conditions. The conditions arise after integrating Eq. (4) across the boundary at $y = -d$ and $y = 0$. These boundary conditions imply the continuity of $\tilde{E}_x$, while $\frac{\partial \tilde{E}_x}{\partial y}$ exhibits a finite discontinuity of $-\frac{4\pi}{c}i\omega m_0 \tilde{N}(\omega)$ and $\frac{4\pi}{c}i\omega m_0 \tilde{N}(\omega)\exp(-\frac{d}{l})$ at the boundaries $y = -d$ and $y = 0$, respectively. In this way, we find the electric field emitted into free space at $y = 0$.

We calculated the spectrum of the emitted electric field and, assuming $d = 100$ μm, $l = 100$ μm [40], $V = c/n_{\text{opt}}$ with $n_{\text{opt}} \approx 2.3$ for $\hbar\omega = 1.55$ eV and $n \approx 2.2$ for $\hbar\omega = 0.97$ eV [21], $n_s = 4.8 + 0.05(\Omega/2\pi) + 0.1(\Omega/2\pi)^2$, where $\Omega/2\pi$ is taken in THz. The latter expression for the refractive index is, in fact, a polynomial that accounts for the dispersion observed in the orthoferrites at the THz frequencies [27].

The spectrum $\tilde{S}(\omega)$ of the signal measured in the experiment is different from the calculated spectrum $\tilde{E}_x(\omega, y = 0)$ because of the propagation effects and spectral selectivity of the

spectrometer,

$$\tilde{S}(\omega) = Q_{\text{prop}}(\omega) Q_{\text{det}}(\omega) \tilde{E}_x(\omega, y=0), \qquad (6)$$

where $Q_{\text{prop}}(\omega)$ describes the transformation of the spectrum due to the propagation from the emitting sample to the detecting ZnTe crystal and Q_{det} is the response function of the ZnTe detector [41]. Based on the theory of Ref. [42], we calculated the propagation filter function $Q_{\text{prop}}(\omega)$ for our experiment, taking the geometrical parameters of our spectrometer. The response function for ZnTe was calculated using the theory of Ref [43]. With these functions at hand, we calculated the spectra of the THz signal at the detector generated by the photo-induced magnetization as shown in Fig. 1.

We attribute the slight differences in the spectra obtained for the pump photon energies 1.55 and 0.97 eV, as shown in Figs. 1(d) and 1(e), to the difference in the excitation spot radius since the beam waist changes significantly after the transformation in the optical parametric amplifier. For calculations, we used the spot radius $r = 1.8$ mm and $r = 1.45$ mm for the pump photon energies 1.55 eV and 0.97 eV, correspondingly. Note that the group velocity of the pump pulse inside the material is also slightly different.

Our model correctly predicts the bandwidth of the THz spectrum and the positions of the Fabry-Perot peaks. Despite the crudeness of the approximations that we used, the agreement between the theory and the experiment is rather good.

From the measured strength of the electric field, we estimate the amplitude of the emitting magnetization $m_0 \approx 0.06$ emu/cm^3. This is about 0.6% of the net magnetization, $M_S \approx 10$ emu/cm^3.

D. Microscopic origin of the photo-induced magnetization

Using first- and second-order perturbation theories as well as following the procedure similar to that described in [44,45], we performed a quantum mechanical analysis of the interaction of light with Dy^{3+} ions. If the lifetime of the electrons in the excited state is much longer than the pulse duration, the second-order effects are small. The origin of the photo-induced magnetization in the first-order perturbation theory is a result of photogeneration of Frenkel's excitons formed by the interaction of $^6H_{15/2}$ holes and $^6H_{9/2}$ electrons. Since the total angular momentum must be conserved, in isotropic media an exciton generated via absorption of circularly polarized light must have a magnetic moment parallel or antiparallel to the wave vector of light. The polarity of the magnetic moment is defined by the light helicity and the absolute value of the moment must be equal to $2\mu_B$, where μ_B is the Bohr magneton. The macroscopic optically induced magnetization is thus proportional to the probability of the exciton generation $P(t)$,

$$P(t) = \Sigma_{j,i} \frac{2\pi}{\hbar} |\langle \Psi_j | \widehat{V}(t) | \Psi_i \rangle|^2 \Gamma_i^{-1} \rho_j, \qquad (7)$$

where $\widehat{V}(t)$ is the perturbation, Ψ_j is the wave function of the j state of the ground multiplet $^6H_{15/2}$, Ψ_i is the wave function of the i state of the excited multiplet $^6H_{9/2}$, Γ_i^{-1} is the spectral width of the excited i state, and ρ_j is the occupation probability of the ground k state. Under the assumption that the time of optical decoherence ΔT for the excitation from the ground $^6H_{15/2}$ to the excited multiplet $^6H_{9/2}$ is short compared to the period of the paramagnetic resonance of the Dy^{3+} ions, for the photo-induced magnetization, one obtains

$$m = \pm 2\mu_B P(t) \Delta T, \qquad (8)$$

where the sign is defined by the a helicity of light. Γ_i^{-1} as well as ρ_j for the lowest states decrease upon temperature increase, which explains the temperature dependence of the photo-induced magnetization observed in the experiment.

IV. CONCLUSION

To conclude, we showed that femtosecond resonant pumping of Dy^{3+} ions in multisublattice $DyFeO_3$ triggers THz dynamics of their magnetization, leading to an emission of broadband THz radiation. This process competes with the off-resonant excitation of the spin waves in the Fe^{3+} subsystem via the inverse Faraday effect. It is interesting to note that our experiments reveal a possibility of magnetometry with elemental specificity. The magnetization of Fe mainly contributes to the narrowband component of the THz radiation at the frequency of the antiferromagnetic resonance. The contribution from Dy is broadband and has temperature dependence following the Curie-Weiss law, being the strongest at low temperatures and hardly visible at room temperature. Analyzing the spectrum and temperature dependencies, one can clearly distinguish between the magnetization dynamics of Fe and Dy. Finally we would like to note that the strength of the electric field of the broadband THz generation in our experiment reaches 10 V/cm so that the efficiency of the THz generation normalized to the sample thickness is just one order of magnitude smaller than that of ZnTe. However, since the group velocity of the optical pulse in $DyFeO_3$ is larger than the phase velocity of light at THz frequencies [21,46], a significant enhancement of the emitted THz waves employing the Cherenkov effect [47,48] is quite possible.

[1] A. Kirilyuk, A. V. Kimel, and Th. Rasing, Rev. Mod. Phys. **82**, 2731 (2010).

[2] I. Žutić, J. Fabian, and S. Das Sarma, Rev. Mod. Phys. **76**, 323 (2004).

[3] V. V. Kruglyak, S. O. Demokritov, and D. Grundler, J. Phys. D: Appl. Phys. **43**, 264001 (2010).

[4] T. Kubacka *et al.*, Science **343**, 1333 (2014).

[5] E. Beaurepaire, J.-C. Merle, A. Daunois, and J.-Y. Bigot, Phys. Rev. Lett. **76**, 4250 (1996).

[6] Y. R. Shen and N. Bloembergen, Phys. Rev. **143**, 372 (1966).

[7] P. S. Pershan, J. P. van der Ziel, and L. D. Malmstrom, Phys. Rev. **143**, 574 (1966).

[8] A. V. Kimel, A. Kirilyuk, P. A. Usachev, R. V. Pisarev, A. M. Balbashov, and Th. Rasing, Nature (London) **435**, 655 (2005).

[9] R. Iida, T. Satoh, T. Shimura, K. Kuroda, B. A. Ivanov, Y. Tokunaga, and Y. Tokura, Phys. Rev. B **84**, 064402 (2011).

[10] A. V. Kimel, C. D. Stanciu, P. A. Usachev, R. V. Pisarev, V. N. Gridnev, A. Kirilyuk, and Th. Rasing, Phys. Rev. B **74**, 060403 (2006).

[11] J. A. de Jong, A. V. Kimel, R. V. Pisarev, A. Kirilyuk, and Th. Rasing, Phys. Rev. B **84**, 104421 (2011).

[12] F. Hansteen, A. Kimel, A. Kirilyuk, and Th. Rasing, Phys. Rev. Lett. **95**, 047402 (2005).

[13] T. Satoh *et al.*, Nat. Photon. **6**, 662 (2012).

[14] A. M. Kalashnikova, A. V. Kimel, R. V. Pisarev, V. N. Gridnev, A. Kirilyuk, and Th. Rasing, Phys. Rev. Lett. **99**, 167205 (2007).

[15] T. Satoh, S.-J. Cho, R. Iida, T. Shimura, K. Kuroda, H. Ueda, Y. Ueda, B. A. Ivanov, F. Nori, and M. Fiebig, Phys. Rev. Lett. **105**, 077402 (2010).

[16] N. Kanda *et al.*, Nat. Commun. **2**, 362 (2011).

[17] J. Nishitani, T. Nagashima, and M. Hangyo, Appl. Phys. Lett. **103**, 081907 (2013).

[18] D. Bossini, A. M. Kalashnikova, R. V. Pisarev, Th. Rasing, and A. V. Kimel, Phys. Rev. B **89**, 060405 (2014).

[19] L. Chaix, S. de Brion, S. Petit, R. Ballou, L.-P. Regnault, J. Ollivier, J.-B. Brubach, P. Roy, J. Debray, P. Lejay, A. Cano, E. Ressouche, and V. Simonet, Phys. Rev. Lett. **112**, 137201 (2014).

[20] D. Bossini, D. Malik, B. Redlich, A. F. G. van der Meer, R. V. Pisarev, Th. Rasing, and A. V. Kimel, Phys. Rev. B **87**, 085101 (2013).

[21] P. A. Usachev *et al.*, Phys. Solid State **47**, 2292 (2005).

[22] A. K. Zvezdin and V. M. Matveev, Sov. Phys. JETP **50**, 543 (1979).

[23] *Terahertz Spectroscopy. Principles and Applications*, edited by S. L. Dexheimer (CRS, Boca Raton, FL, 2007).

[24] E. Beaurepaire, G. M. Turner, S. M. Harrel, M. C. Beard, J. Y. Bigot, and C. A. Schmuttenmaer, Appl. Phys. Lett. **84**, 3465 (2004).

[25] D. J. Hilton, R. D. Averitt, C. A. Meserole, G. L. Fisher, D. J. Funk, J. D. Thompson, and A. J. Taylor, Opt. Lett. **29**, 1805 (2004).

[26] T. Kampfrath, M. Battiato, P. Maldonado, G. Eilers, J. Notzold, S. Mahrlein, V. Zbarsky, F. Freimuth, Y. Mokrousov, S. Blügel, M. Wolf, I. Radu, P. M. Oppeneer, and M. Munzenberg, Nat. Nanotechnol. **8**, 256 (2013).

[27] Z. Jin, Z. Mics, G. Ma, Zh. Cheng, M. Bonn, and D. Turchinovich, Phys. Rev. B **87**, 094422 (2013).

[28] R. R. Birss, *Symmetry and Magnetism* (North-Holland, Amsterdam, 1966).

[29] M. Fiebig, V. V. Pavlov, and R. V. Pisarev, J. Opt. Soc. Am. B **22**, 96 (2005).

[30] A. Kirilyuk, V. V. Pavlov, R. V. Pisarev, and Th. Rasing, Phys. Rev. B **61**, R3796 (2000).

[31] V. N. Gridnev, V. V. Pavlov, R. V. Pisarev, A. Kirilyuk, and Th. Rasing, Phys. Rev. B **63**, 184407 (2001).

[32] A. Kastler, J. Opt. Soc. Am. **47**, 460 (1957).

[33] R. Kolesov, Phys. Rev. A **76**, 043831 (2007).

[34] O. Nikolov, T. Ruskov, T. Tomov, A. M. Kadomtseva, I. B. Krinetskii, and M. M. Lukina, J. Magn. Magn. Mater. **44**, 181 (1984).

[35] W. J. Tabor, A. W. Anderson, and L. G. Van Uitert, J. Appl. Phys. **41**, 3018 (1970).

[36] *Numerical Data and Functional Relationships*, Landolt-Boernstein New Series Group III, edited by H. P. J. Wijn (Springer, Berlin, 1981), Vol. 27 f3, pp. 125–134.

[37] R. V. Mikhaylovskiy *et al.*, Nat. Commun. **6**, 8190 (2015).

[38] R. V. Mikhaylovskiy, E. Hendry, V. V. Kruglyak, R. V. Pisarev, Th. Rasing, and A. V. Kimel, Phys. Rev. B **90**, 184405 (2014).

[39] H. Schuchert *et al.*, Z. Phys. **220**, 273 (1969).

[40] D. E. Wood *et al.*, J. Appl. Phys. **41**, 5315 (1970).

[41] T. J. Huisman, R. V. Mikhaylovskiy, A. Tsukamoto, Th. Rasing, and A. V. Kimel, Phys. Rev. B **92**, 104419 (2015).

[42] M. A. Khazan and J. Kroupa, J. Opt. Soc. Am. B **16**, 1795 (1999).

[43] G. Gallot, J. Zhang, R. W. McGowan, T.-I. Jeon, and D. Grischkowsky, Appl. Phys. Lett. **74**, 3450 (1999).

[44] D. Popova, A. Bringer, and S. Blügel, Phys. Rev. B **84**, 214421 (2011).

[45] D. Popova, A. Bringer, and S. Blügel, Phys. Rev. B **85**, 094419 (2012).

[46] *High Frequency Processes in Magnetic Materials*, edited by G. Srinivasan and A. N. Slavin (World Scientific, Singapore, 1995).

[47] M. I. Bakunov, R. V. Mikhaylovskiy, and S. B. Bodrov, Phys. Rev. B **86**, 134405 (2012).

[48] S. D. Gorelov, E. A. Mashkovich, M. V. Tsarev, and M. I. Bakunov, Phys. Rev. B **88**, 220411(R) (2013).